Microporous Polyimides with Uniform Pores for Adsorption and Separation of CO2 Gas and Organic Vapors

ARTICLE *in* MACROMOLECULES · APRIL 2013

Impact Factor: 5.8 · DOI: 10.1021/ma400496q

2 AUTHORS, INCLUDING:

Zhonggang Wang
Dalian University of Technology
499 PUBLICATIONS **10,225** CITATIONS

Macromolecules

Article

pubs.acs.org/Macromolecules

Microporous Polyimides with Uniform Pores for Adsorption and Separation of CO_2 Gas and Organic Vapors

Guiyang Li and Zhonggang Wang*

State Key Laboratory of Fine Chemicals, Department of Polymer Science and Materials, School of Chemical Engineering, Dalian University of Technology, Dalian 116024, China

Supporting Information

ABSTRACT: Three microporous polyimides, MPI-1, MPI-2, and MPI-3, with uniform pores were synthesized via one-pot polycondensation from tetrakis(4-aminophenyl)methane, tris(4-aminophenyl)amine and 1,3,5-tris(4-aminophenyl)benzene with pyromellitic dianhydride, respectively. The amorphous networks exhibit excellent thermal stability, large BET surface areas up to 1454 $m^2\ g^{-1}$, and narrow pore size distribution in the range from 5 to 6 Å. Their adsorption−desorption isotherms of CO_2 are reversible, and the CO_2 uptakes at 273 K and 1 bar are up to 16.8 wt %. Moreover, based on the ratios of initial slopes of isotherms, the CO_2/N_2 and CO_2/CH_4 separation factors are as high as 102 and 12, respectively. The above CO_2 adsorption and separation properties are attributed to the presence of abundant electron-rich heteroatoms in the polyimide networks and the unifrom ultralmicroporous structures. In addition, for MPI-1, the adsorption capacity of benzene vapor is 119.8 wt %, while the separation factors of benzene over nitrogen and water reach 342 and 28, respectively. The outstanding selective adsorptions of CO_2 gas and benzene vapor endow the microporous polyimides with promising potential in CO_2 capture and separation as well as air- and water-cleaning applications.

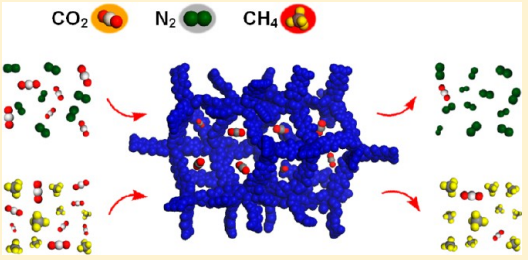

INTRODUCTION

Carbon dioxide (CO_2) capture and storage is a newly emerged technology with promising potentials in the reduction of greenhouse gas and purification of nature gas. CO_2 gas, mainly produced from the burning of fossil fuels and biomass, is regarded as a culprit for global-warming. Usually, the flue gas of post-combustion from coal-fired power plants is composed of 15−16% CO_2, 70−75% N_2, 5−7% water vapor, and some other impurities,[1] whereas the pre-combustion gases, e.g., natural gas and landfill gas, contain as high as 5−20% and 40−60% CO_2 contaminant, respectively, which has to be removed to facilitate sufficient burning.[2] On the other hand, as an important chemical material and reaction medium, the recovered CO_2 can be utilized in the syntheses of numerous polymers and fine chemicals such as polycarbonates,[3] cyclic carbonate,[4] dimethyl ether,[5] and methylacrylic acid.[6] In this regard, developing porous adsorbents with large surface area, high CO_2 adsorption capacity, excellent CO_2/N_2 and CO_2/CH_4 selectivities is of significance for both academic study and industrial applications.

Aqueous solutions of amines such as ethanolamine have been widely employed to absorb CO_2, but the subsequent process for the regeneration of amine and recovery of CO_2 is rather energy-consuming.[7] As an alternative method, the physical sorption of CO_2 by porous solid materials with large surface area are receiving attention, including porous zeolites,[8] metal−organic frameworks,[9] and microporous organic polymers.[10] Recently, some results for CO_2 adsorption in microporous organic polymers have been reported.[11] At high pressure, the saturation uptakes of CO_2 in porous polymer networks can reach high level. However, at low pressure region, e.g., in the case of practical CO_2 capture for post-combustion flue gas, the CO_2 capacities are not satisfactory because of the lack of strong affinity toward CO_2 molecule. Therefore, the current efforts are made to incorporate polar groups onto microporous frameworks through post-modification method or directly synthesize micoroporous polymers using the nitrogen- and oxygen-rich monomers. In this way, CO_2 adsorption capability and isosteric heat of adsorption can be enhanced by means of the dipole−quadrupole interactions or hydrogen-bonding effect between pore wall and CO_2 molecule. Cooper and co-workers found that, at 273 K and 1 bar, the network-A only composed of aromatic benzene rings could uptake CO_2 of 2.65 mmol g^{-1}. After inserting a triazole ring between two phenyls, the network-C exhibited remarkably improved CO_2 uptake up to 3.86 mmol g^{-1}.[12] The other successful examples are polyamine and sulfonate-grafted PPN-6s,[13] oxygen-rich phloroglucinol-based porous polymers,[14] nitrogen-rich microporous polybenzimidazoles,[15] nitrogen- and oxygen-rich microporous cyanate resins,[16] etc.

In parallel to CO_2 capture, the recovery and selective removal of toxic organic vapors from air and water are equally important since the chemical pollutants in working and life environments, emitted from synthetic industry and chemical products such as paints, varnishes, and chemical cleaners, are seriously harmful

Received: March 8, 2013
Revised: March 22, 2013
Published: April 1, 2013

to human health even though at a low concentration. Nevertheless, relative to the studies on CO_2 capture, less attention has been paid to the adsorption of organic vapors. Only very recently, its significance is being emphasized owing to the growing demands for air and water-cleaning as well as the recovery of organic chemicals.[15d,16,17] Langsam and Robeson reported that poly(TMSP) with large free volume were effective to remove chloroform and toluene from water.[18] The wholly aromatic microporous polymers also have promising potential for this purpose, in particular for aromatic compounds, due to the $\pi-\pi$ interaction between phenyls and benzene rings.

In the past years, linear polyimides with intrinsic microporosity and hypercrosslinked microporous polyimide networks have been reported.[19] Among them, the microporous polyimides with three-dimensional network structure have aroused great interest because of the extremely rigid heteroaromatic skeleton and excellent resistance to high temperature and aggressive chemicals. Moreover, the presence of abundant nitrogen and oxygen atoms from the imide rings may lead to polyimide networks the favorable interaction with CO_2 gas. Some interesting data of gas and vapor adsorptions in microporous polyimides have appeared in the literature. For example, the tetraphenyladmantane-based microporous polyimide can uptake 14.6 wt % CO_2 at 273 K and 1 bar, 99.2 wt % benzene and 59.7 wt % cyclohexane at 298 K and 0.9 bar.[19g] However, up to now, systematical studies on synthesis, pore structure, chemical composition and their correlations with adsorptions and separations of CO_2 gas and organic vapors for microporous polyimides are rarely reported. In addition, the pore sizes in many previous materials are relatively wide, which are disadvantageous for the separation of gases. The motivation of the present work, therefore, is to prepare series of microporous polyimides with uniform pore size through elaborately optimizing the polymerization process. Their adsorptions of CO_2 gas and organic vapors as well as the separations of CO_2/N_2, CO_2/CH_4, CO_2/H_2O, benzene/N_2, and benzene/H_2O were evaluated and investigated in term of the porosity parameters, chemical structure and composition of the polymer networks.

EXPERIMENTAL SECTION

Materials. Tetraphenylmethane, tris(4-nitrophenyl)amine, 4-nitroacetophenone, and pyromellitic dianhydride (PMDA) were purchased from J&K Chemical Co., Ltd. PMDA was purified by sublimation prior to use. *m*-Cresol, isoquinoline, and other reagents were purchased from Shanghai Chemical Reagent Co. *m*-Cresol was purified by distillation under reduced pressure and dehydrated with 4A molecular sieves. Tetrahydrofuran (THF) was purified by refluxing over sodium with the indicator benzophenone complex. Isoquinoline, fuming nitric acid, acetic acid, acetic anhydride, and other reagents were of reagent grade and used as received.

Instrumention. Fourier transform infrared spectra (FTIR) of synthesized products were recorded using a Nicolet 20XB FT-IR spectrophotometer in 400−4000 cm^{-1}. Samples were prepared by dispersing the complexes in KBr to form disks. ^1H NMR spectra were recorded on a 400 MHz Varian INOVA NMR spectrometer, using tetramethylsilane as an internal standard. Solid-state ^{13}C CP/MAS (cross-polarization with magic angle spinning) spectra were measured on a Varian Infinity-Plus 400 spectrometer at 100.61 MHz at an MAS rate of 10.0 kHz using zirconia rotors 4 mm in diameter using a contact time of 4.0 ms and a relaxation delay of 2.0 s. Elemental analyses were determined with an Elementar Vario EL III elemental analyzer. Wide-angle X-ray diffractions (WAXD) from 5° to 60° were performed on Rigku D/max-2400 X-ray diffractometer (40 kV, 200 mA) with a copper target at a scanning rate of 2°/min. Field-emission scanning electron microscopy (FE-SEM) experiments were carried on a Nova NanoSEM 450. Before measurement, the samples were sputter-coated with chromium film to facilitate conduction. Transmission electron microscopy (TEM) images were obtained on a Hitachi HT-7700 operated at 100 kV. Thermogravimetric analysis curves were recorded on a NETZSCH TG 209 thermal analyzer by heating the samples (~8 mg) up to 800 °C with ramping rate of 10 °C min^{-1} under nitrogen flow. Adsorption and desorption measurements for all the gases and vapors were conducted on an Autosorb iQ (Quantachrome) analyzer. Prior to measurements, the samples were degassed at 150 °C under high vacuum overnight. Adsorption and desorption isotherms of nitrogen were measured at 77 K. The surface areas were calculated according to the Brunauer−Emmett−Teller (BET) model in the relative pressure (P/P_0) range from 0.07 to 0.15 for MPI-1, from 0.12 to 0.20 for MPI-2, and from 0.05 to 0.12 for MPI-3. CO_2 and CH_4 adsorption isotherms were measured at 273 K up to 1.0 bar. The adsorptions of benzene, cyclohexane and water vapors were measured with the pressure up to the saturated vapor pressure at 298 K. N_2 adsorption isotherms at 273 and 298 K were measured in order to evaluate the adsorption selectivities of CO_2/N_2, CO_2/CH_4, benzene/N_2, and benzene/water, which were calculated from the ratios of initial slopes of pure-component sorption isotherms of gases and vapors.

Synthesis of Tetrakis(4-nitrophenyl)methane (TNPM). Tetraphenylmethane (7.4 g, 23.09 mmol) was added into fuming nitric acid (40 mL) at −40 °C under vigorous stirring. Then, acetic anhydride (12.5 mL) and acetic acid (25 mL) were slowly added and stirred for 1 h. After filtration, the resulted yellow solid was recrystallized with THF to give yellow crystals. Yield: 65%. Mp: 339 °C; ^1H NMR (400 MHz, $CDCl_3$): δ (ppm) 8.22−8.25 (d, 8H, Ar−H), 7.60−7.62 (d, 8H, Ar−H). FTIR (KBr, cm^{-1}): 3070, 3100, 1605, 1591, 1519, 1493, 1347, 840, 757, 744, 711.

Synthesis of Tetrakis(4-aminophenyl)methane (TAPM). TAPM was prepared in reference to the procedure in ref 20 with some modifications. In a hydrogenator, dry tetrahydrofuran (40 mL), TNPM (1.6 g, 3.19 mmol) and catalysis amount of Pd/C was added and purged with nitrogen. Then, the mixture was stirred under 1.2 MPa hydrogen pressure at room temperature for 3 days. After removing the Pd/C powder and solvent, the white product was purified by recrystallization. Yield: 95%. Mp: 262 °C; ^1H NMR (400 MHz, DMSO-d_6): δ (ppm) 6.66−6.68 (d, 8H, Ar−H), 6.38−6.40 (d, 8H, Ar−H), 4.85 (s, 8H, $-NH_2$). FTIR (KBr, cm^{-1}): 3442, 3400, 3363, 3333, 3027, 3100, 1620, 1508, 1281, 1216, 1184, 820, 754, 577; HRMS calculated for $C_{25}H_{24}N_4$, 380.2001; found, 380.2004.

Synthesis of Tris(4-aminophenyl)amine (TAPA). TAPA was prepared by a procedure similar to that for TAPM except that the precursor compound is tris(4-nitrophenyl)amine instead of tetrakis(4-nitrophenyl)methane. Yield: 90%. Mp: 241 °C; ^1H NMR (400 MHz, DMSO-d_6): δ (ppm) 6.60−6.62 (d, 6H, Ar−H), 6.46−6.44 (d, 6H, Ar−H), 4.68 (s, 6H, $-NH_2$). FTIR (KBr, cm^{-1}): 3411, 3340, 3029, 1622, 1504, 1262.

Synthesis of 1,3,5-Tris(4-nitrophenyl)benzene (TNPB). TNPB was prepared in reference to the literature[21] with some modifications. 4-Nitroacetophenone (25.1 g, 0.15 mol) and anhydrous ethanol (43.7 mL, 0.75 mmol) were charged in a three-necked flask equipped with a magnetic stirrer. Thionyl chloride (18.2 mL, 0.25 mol) was added dropwise. Then the mixture was reacted at the refluxing temperature for additional 1 h. The solid was neutralized and washed successively with deionized water, ethyl ether, and ethanol. The crude product was recrystallized with DMF to give yellow needle-like solid. Yield: 77%. Mp: 325 °C. ^1H NMR (400 MHz, DMSO-d_6): δ (ppm) 8.38−8.36 (d, 6H, Ar−H), 8.27−8.29 (6H, Ar−H), 8.26 (3H, Ar−H). FTIR (KBr, cm^{-1}): 1594, 1511, 1349, 862, 843, 629.

Synthesis of 1,3,5-Tris(4-aminophenyl)benzene (TAPB). TAPB was prepared by a similar procedure to TAPM. Yield 95%. Mp: 262 °C; ^1H NMR(400 MHz, acetone-d_6): δ (ppm) 7.59 (s, 3H, Ar−H), 7.51−7.53 (d, 6H, Ar−H), 6.77−6.79 (d, 6H, Ar−H), 4.76 (6H, -NH_2); ^{13}C NMR (100 MHz, acetone-d_6): δ (ppm) 149.0, 143.1,

dx.doi.org/10.1021/ma400496q | Macromolecules 2013, 46, 3058−3066

Scheme 1. Synthesis Routes to the Three Polyimide Networks

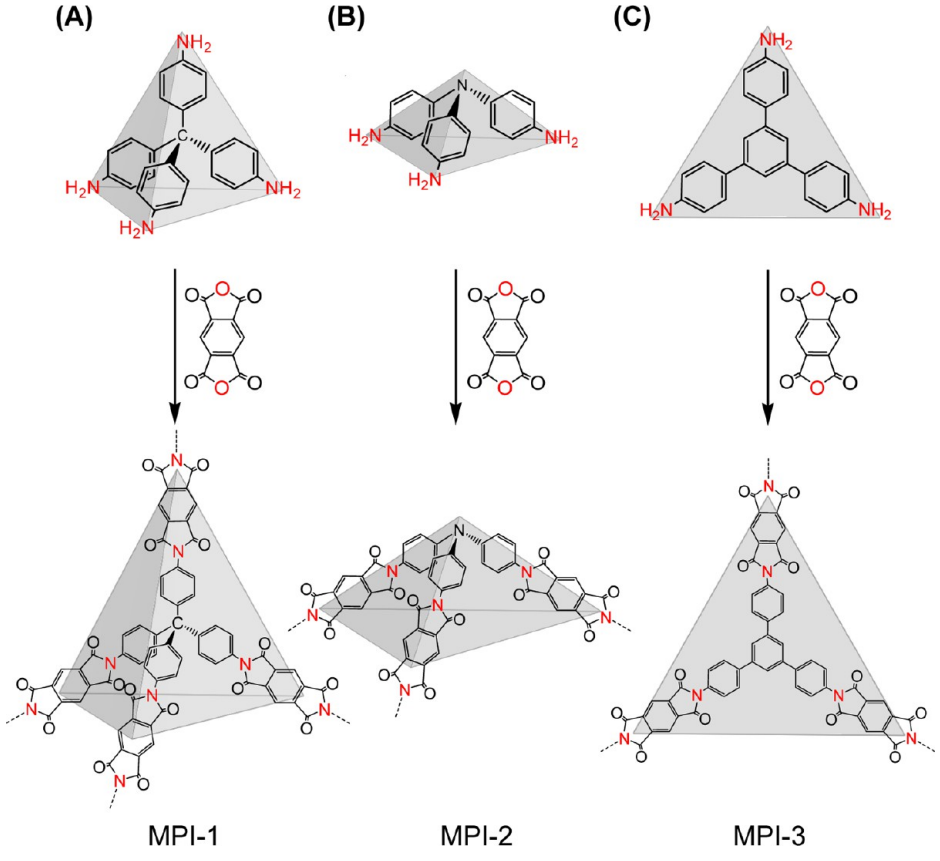

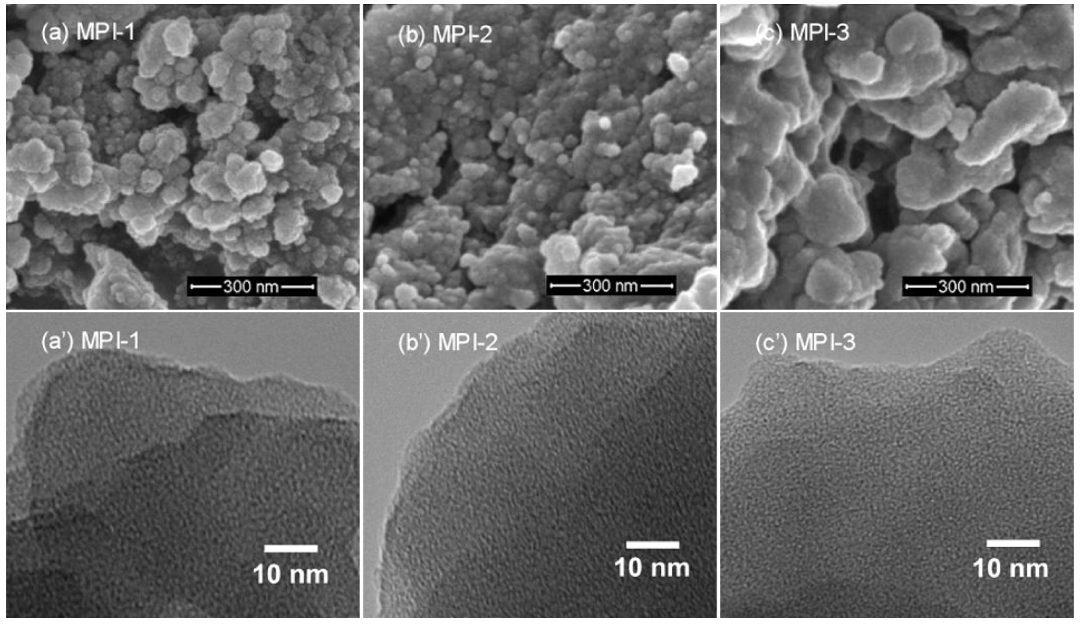

Figure 1. SEM images of MPI-1 (a), MPI-2 (b), and MPI-3 (c); HR-TEM images of MPI-1 (a′), MPI-2 (b′) and MPI-3 (c′).

130.7, 128.9, 122.3, 115.5. FTIR (KBr, cm^{-1}): 3442, 3360, 1620, 1593, 1516, 1283, 827.

Preparation of Polyimide Networks. The polymerizations of MPI-1, MPI-2, and MPI-3 were carried out in similar procedures. Only the polymerization of MIP-1 is described here as an example. A dry Schlenk flask equipped with a stirrer, a condenser, and an ice-bath was degassed using two evacuation−argon backfill cycles. Under argon flow, TAPM (0.40 g, 1.38 mmol), PMDA (0.45 g, 2.07 mmol), and 10 mL *m*-cresol were added and stirred for 2 h. After the reaction was slowly heated to room temperature, a catalytical amount of isoquinoline was added. Then the temperature of polymerization was raised in the heating schedule: 30 °C for 8 h, 80 °C for 4 h, 160 °C for 4 h, 200 °C for 10 h, and 220 °C for 4 h. Finally, the system was cooled down, and the solid was isolated and washed successively with DMF, methanol, and THF. The resultant product was extracted with THF in a Soxhlet apparatus for 24 h, and dried at 120 °C under

dx.doi.org/10.1021/ma400496q | *Macromolecules* 2013, 46, 3058−3066

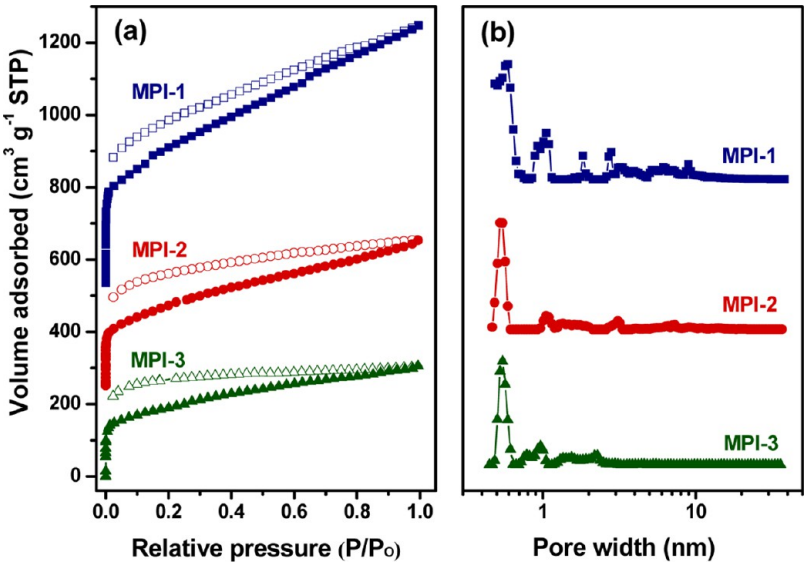

Figure 2. (a) Adsorption (filled) and desorption (empty) isotherms of N_2 for MPI-1 (+600), MPI-2 (+300), and MPI-3. (b) Pore size distribution curves for MPI-1, MPI-2, and MPI-3.

vacuum to constant weight. Quantitative yield was achieved in every case.

RESULTS AND DISCUSSION

Synthesis and Porous Structure of Polyimide Networks. Using *m*-cresol as reaction medium and isoquinoline as catalyst, the condensation polymerizations of pyromellitic dianhydride (PMDA) with tetra(4-aminophenyl)methane (TAPM), 1,3,5-tris(4-aminophenyl)benzene (TAPB) and tris-(4-aminophenyl)amine (TAPA) led to three polyimide networks MPI-1, MPI-2 and MPI-3, respectively (Scheme 1).

In FTIR spectra (Figure S1, Supporting Information), the structures of polyimides are confirmed by the characteristic bands at 1779 and 1726 cm^{-1} due to the symmetric and asymmetric vibrations of the C═O group, and that at 1349 cm^{-1} corresponding to the stretching vibration of the C−N−C moiety of five-member imide ring. Meanwhile, the absorptions of amino and anhydride in monomers are absent, indicating that the reactive groups have been completely converted under the polymerization conditions. In solid-state ^{13}C CP/MAS NMR spectra (Figure S2, Supporting Information), the resonance of carbonyl carbon in imide ring appears at 165 ppm. The quaternary carbon in MPI-1 locates at 20 ppm, and the N-substituted phenyl carbon for MPI-2 is at 146 ppm. The overlapping signals from 121 to 137 ppm belong to the other aromatic carbons in backbone. Elemental analyses show that the measured chemical compositions are consistent with the calculated values (Table S1, Supporting Information) except for hydrogen and nitrogen. The slightly higher hydrogen and lower nitrogen contents than the theoretical values may be caused by the absorbed moisture and CO_2 from air.

For each sample, the resultant brown solid can not dissolve in any solvents, suggesting the hypercrosslinked structure. The thermal stabilities of three samples were evaluated by thermogravimetric analysis (TGA) under a nitrogen atmosphere (Figure S3, Supporting Information). The weight losses corresponding to the decomposition of skeleton occur at over 530 °C, and the char yields at 800 °C are 57.4, 53.0, and 59.3 wt % for MPI-1, MPI-2, and MPI-3, respectively. The small weight-losses at around 240 °C are possibly caused by the solvent and catalyst entangled in the microporous networks.

The surface morphologies of the products were observed by field-emission scanning electron microscopy (Figure 1a−c). Similar to other microporous polymers,[22] the samples are homogeneous, composing of loose agglomerates of tiny particles with rough surface and irregular shape. The pore morphology and pore size of the three samples were examined by a high-resolution transmittance electron microscopy (TEM in Figure 1a′-1c′). For the sake of clarity, the enlarged TEM images are presented in Figure S4−S6, Supporting Information. The white region corresponds to the nanopore channels, while the dark region is attributed to the polyimide skeleton. As can be seen, the pores in all the three polyimides are uniform with the width of pore channel at around 0.5 nm.

The porosity parameters of polyimide networks were investigated by physical sorption of nitrogen at 77 K (Figure 2a). The isotherms displayed rapid nitrogen uptake at the very low relative pressure (<0.01), indicative of the characteristics of permanent micropores. In this study, three monomers with different geometry configurations were selected as the building blocks. TAPM has a tetrahedral shape with four phenyls stretching outward from a sp^3-hybridized carbon core. The three-dimensional network with tetraphenylmethanes linked by rigid imide rings is liable to generate large amount of pores. Indeed, MPI-1 exhibits the BET surface area, Langmuir surface area and total pore volume of 1454 $m^2\ g^{-1}$, 2116 $m^2\ g^{-1}$, and 1.07 $cm^3\ g^{-1}$, respectively, which are the highest among the three polymers (Table 1). In contrast, the planar-triangular shape of TAPB makes the polymer incline to form two-dimensional network. The $\pi-\pi$ stacking between layers may

Table 1. Porosity Parameters of the Polyimide Networks Obtained by N_2 Adsorption

samples	monomers	S_{BET} ($m^2\ g^{-1}$)	$S_{Langmuir}$ ($m^2\ g^{-1}$)	V_{total} ($cm^3\ g^{-1}$)	pore size (nm)
MPI-1	TAPM + PMDA	1454	2116	1.07	0.59
MPI-2	TAPA + PMDA	814	1185	0.59	0.52
MPI-3	TAPB + PMDA	586	842	0.31	0.55

dx.doi.org/10.1021/ma400496q | Macromolecules 2013, 46, 3058−3066

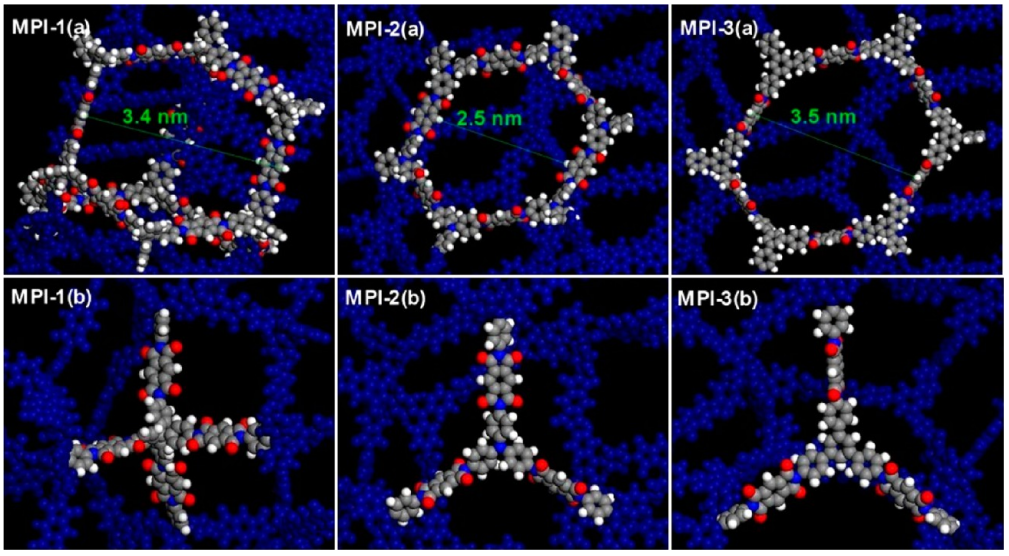

Figure 3. Energy-optimized molecule models for MPI-1 (left), MPI-2 (middle), and MPI-3 (right): (a) obtained from an ideal linking mode; (b) obtained from a randomly interpenetrating mode.

lead to the loss of pore. As a result, MPI-3 shows apparently lower BET surface area of 586 $m^2\ g^{-1}$ and pore volume of 0.31 $cm^3\ g^{-1}$. The topological structure of MPI-2 constructed from the nitrogen-centered TAPA monomer with triangular-pyramidal shape lies between MPI-1 and MPI-3, and consequently, MPI-2 has a modest BET surface area of 814 $m^2\ g^{-1}$.

The pore size distributions obtained by the nonlocal density functional theory (NLDFT) are illustrated in Figure 2b. It is interesting to observe that, although the WAXD curves indicate that the three polymer networks are amorphous (Figure S7, Supporting Information), their pore sizes are quite uniform, centering at around 0.59, 0.52, and 0.55 nm for MPI-1, MPI-2, and MPI-3, respectively, which are well consistent with the observations in TEM images. In order to elucidate the possible pore-forming mechanism, molecular simulations were carried out using Materials Studio software. At first, the molecular models were built assuming that the cross-linking reactions are complete and all the reactive groups are linked in an ideal mode according to the geometrical structure of monomer. After being optimized by geometry and molecular mechanics successively, and then relaxed through dynamic calculation at 298 K for 200 ps based on the COMPASS force field, the polymer networks present the network topologies as illustrated in Figure 3a, in which the pore sizes of MPI-1, MPI-2 and MPI-3 are 3.4, 2.5, and 3.5 nm, respectively, far larger than the experimental values.

The above results indicate that the interpenetration of networks during the synthesis of polyimides can not be ignored since the polycondensations between polyamine and dianhydride monomers are kinetically controlled, following the step-polymerization mechanism. The whole process successively undergoes several stages including oligomerization, branching, gelation and the eventual formation of hypercrosslinked network. Similar to the case of microporous polyarylates,[23] under the controlled conditions, the polyamine monomer and PMDA first react to yield hyperbranched precursor. Subsequently, upon gradually heating the system to a higher temperature, the long branches of the precursors start to randomly cross-link with each other. Thus, the larger mesopores shown in Figure 3a are homogeneously divided into ultramicropores (<7 Å) by the interpenetrated segments as depicted in Figure 3b.

Adsorption of Organic and Water Vapors in Polyimide Networks. The adsorption isotherms of benzene, cyclohexane and water vapors measured at 298 K are presented in Figure 4. In contrast to cyclohexane and water, the three

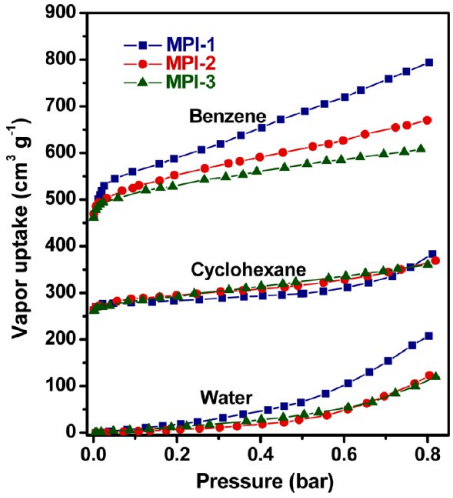

Figure 4. Organic and water vapor adsorption isotherms at 298 K for three polyimide networks (benzene +450, cyclohexane +250, water).

polyimides exhibit a rapid rise of benzene uptake at the low relative pressure (P/P_0 < 0.1), indicating that the wholly aromatic skeleton have a strong affinity toward benzene molecules. The data in Table 2 show that, at P/P_0 = 0.8, the sorption capacity of benzene for MPI-1 can reach 119.8 wt %, which is much higher than carbon material F42C (39.5 wt %),[24] metal azolate framework MAF-2 (20.6 wt %),[25] and microporous cyanate resin CE-1 (58.5 wt %).[16a] Cyclohexane is also an organic vapor, but the lack of $\pi-\pi$ interaction leads to cyclohexane apparently lower uptake in comparison with benzene vapor. In addition, the isotherms for water vapor are typical type III sorption, and its uptake in MPI-1 is only 16.7 wt

dx.doi.org/10.1021/ma400496q | Macromolecules 2013, 46, 3058−3066

Table 2. Uptakes of CO_2 Gas, Organic, and Water Vapors in the Polyimide Networks

	gas adsorption and selectivity[a]				vapor adsorption and selectivity[b]				
sample	CO_2 (wt %)	CO_2/N_2	CO_2/CH_4	CO_2/H_2O	C_6H_6 (wt %)	c-C_6H_{12} (wt %)	H_2O (wt %)	C_6H_6/N_2	C_6H_6/H_2O
MPI-1	16.8	102	8	10.5	119.8	50.1	16.7	342	28
MPI-2	13.8	71	12	5.5	76.6	44.8	9.9	310	13
MPI-3	9.9	41	10	10.9	54.9	41.5	9.6	167	14

[a]Uptakes for CO_2, N_2, and CH_4 were determined at 273 K and 1 bar. The CO_2/N_2 and CO_2/CH_4 selectivities were calculated from initial slopes of pure-component sorption isotherms. The CO_2/H_2O selectivities were calculated from the ratio of uptake of CO_2 at 0.15 bar and 298 K to that of water vapor at 0.05 bar at 298 K. [b]Uptakes for C_6H_6 (benzene vapor), c-C_6H_{12} (cyclohexane vapor) and H_2O (water vapor) were determined at P/P_0 = 0.8 and 298 K. The C_6H_6/N_2 and C_6H_6/H_2O selectivities were calculated from initial slopes of pure-component sorption isotherms.

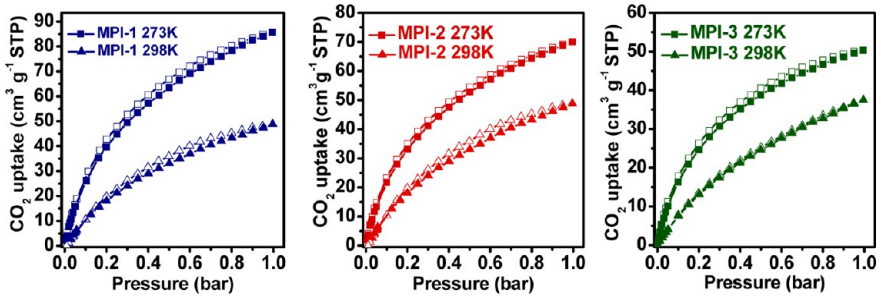

Figure 5. Adsorption (filled) and desorption (empty) isotherms of CO_2 at 273 and 298 K for MPI-1, MPI-2, and MPI-3.

%, indicative of the hydrophobic nature of the polyimide networks.

The separations of benzene vapor from N_2 and H_2O vapor were examined by comparing their initial slopes (Figure S8, Supporting Information). The results reveal that the benzene/N_2 and benzene/H_2O selectivities are as high as 342 and 28, respectively. The high adsorption capacity of benzene and its excellent selectivities over N_2 and water are of significant importance in air and water-cleaning in the environmental protection field.

CO_2 Adsorption and Selectivity of CO_2/N_2 and CO_2/CH_4. The large surface area, ultramicroporous structure and narrow pore size distribution of the polyimides arouse our interest to further explore their property of CO_2 capture and separation from other gases. The sorption isotherms of CO_2 at 273 and 298 K are presented in Figure 5. For all the three samples, the CO_2 uptakes appear a rapid rise in the initial stage, implying that CO_2 molecule has favorable interaction with the polymer skeleton. Moreover, the adsorption−desorption curves of CO_2 are roughly reversible. Thus, the samples can absorb CO_2 gas even on exposure to atmosphere and can release the equivalent amount of CO_2 from their cavity while releasing the pressure, which characteristic is quite desirable for the practical application in CO_2 capture and regeneration of porous adsorbent. Furthermore, it is noted that the uptakes of CO_2 continually increase with the pressure, and have not reached saturation in the experimental range, indicating that the higher adsorption capacity can be achieved at the increased pressure.

MPI-1 has the CO_2 uptake of as high as 16.8 wt % at 1 bar and 273 K (Table 2), which are comparable to that of COFs (5.7−16.7 wt %),[11b,26] CMPs (4.0−17.0 wt %),[22,27] and other microporous polymers.[28] In addition to the large surface area, the excellent CO_2 adsorption performance is probably resulted from the high affinity of skeleton toward CO_2 since polyimide networks contain abundant electron-rich nitrogen and oxygen atoms. To support the above deduction, the isosteric enthalpies (Q_{st}) of MPIs toward CO_2 were calculated from the adsorption isotherms at different temperatures in term of Clausius−Clapeyron equation:[29]

$$\ln p = \frac{Q_{st}}{RT} + C \quad (1)$$

where P, T, R, and C are the pressure, temperature at the equilibrium state, the gas constant, and equation constant, respectively.

The dependencies of CO_2 isosteric enthalpies (Q_{st}) on the adsorbed amount are shown in Figure 6. For each sample, the

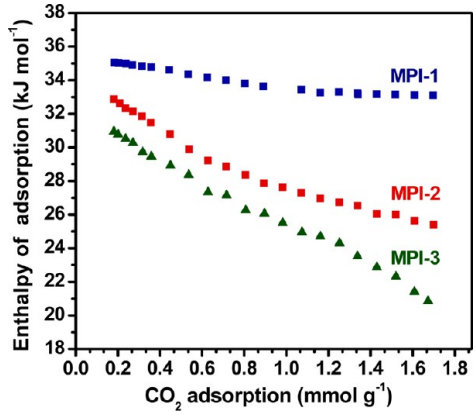

Figure 6. Variation of CO_2 isosteric enthalpies with the adsorbed amount.

Q_{st} values significantly decrease with the adsorbed amount, meaning that the interaction between CO_2 and pore wall is stronger than that between CO_2 molecules. Interestingly, the three polymers have the similar chemical structure but apparently different Q_{st} values. Moreover, the Q_{st} value has the same ranking order as the surface area, pore volume and CO_2 adsorption capacity, implying that, besides the intrinsic affinity of polymer skeleton, the CO_2 capture ability of microporous polymers may also be highly related to the

dx.doi.org/10.1021/ma400496q | Macromolecules 2013, 46, 3058−3066

porosity, topological structure and complexity of pore channels in the network. The combination of the pore structure and affinity between CO_2 and pore wall results in MPI-1 the highest CO_2 uptake among the three polymers.

The physical sorption of CO_2 gas on the polyimide network can also be investigated though the virial equation[30] as below:

$$\ln(n/P) = A_0 + A_1 n + A_2 n^2 + \cdots \quad (2)$$

where n is the adsorbed amount at pressure P, K_H refers to Henry's constant, and A_0, A_1, A_2, etc. are virial coefficients.

At low adsorbed amount of gas, A_2 and higher terms can be neglected. As shown in Figure 7, the virial plots of CO_2 for all the three polymers exhibit good linear relationship. The data of A_0, A_1, and K_H are listed in Table S2, Supporting Information. A_0 is related to the gas-material interaction, whereas A_1 reflects gas-gas interaction. It is seen that MPI-1 has the largest A_0 value, which is consistent with the ranking orders of CO_2 capacities and the isosteric enthalpies obtained by the Clausius–Clapeyron equation.

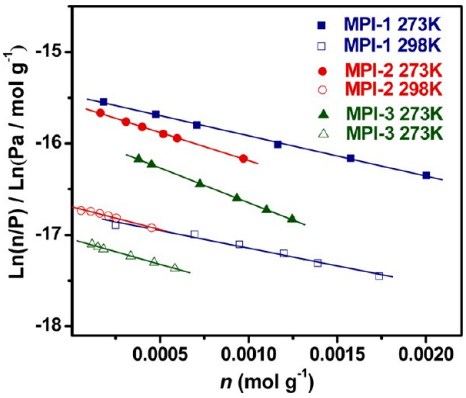

Figure 7. Virial plots of CO_2 adsorption in MPI-1, MPI-2, and MPI-3 at 273 and 298 K.

As the measure of the interaction between CO_2 and pore wall, the enthalpy of adsorption at zero coverage (Q_0) can be calculated using the Vant Hoff equation:

$$\frac{d[\ln K_H]}{dT} = \frac{Q_0}{RT} \quad (3)$$

where Q_0 is the slope of the plot of $\ln(K_H)$ vs $1/T$, while K_H is Henry's constant derived from the equation $K_H = \exp(A_0)$ based on virial plot.

According to the isotherms at different temperatures, the calculated Q_0 values for MPI-1, MPI-2, and MPI-3 are 34.8, 30.4, and 31.4 kJ mol^{-1}, respectively. The values are higher than those of other porous materials like HCPs (20–24 kJmol^{-1}),[31] BILPs (26.5–28.8 kJmol^{-1}),[15c,32] BLPs (20.2–28.3 kJmol^{-1}),[33] and comparable to microporous polymers with organic ammonium ions or Lewis basic amine in pores (30–55 kJmol^{-1}).[34] The exceptionally high Q_0 values can be due to the enhanced affinity for CO_2 molecule because of the abundant N and O atoms as well as the sorption selectivity effects of the ultramicropores[35] in this series of ultramicroporous polyimides.

In order to evaluate the separation property of the polyimides, the sorption isotherms of CH_4 and N_2 at 273 K were measured and are compared with those of CO_2 in Figure 8. The curves show that CO_2 has the considerably higher uptake than N_2 and CH_4 in the whole pressure range. The initial slopes of the CO_2, N_2 and CH_4 based on the adsorption isotherms at 273 K were calculated (Figure S9, Supporting Information), and their ratios of CO_2 over N_2 and CH_4 are used as the separation factors of CO_2/N_2 and CO_2/CH_4 gas pairs.[15c,36] It is known that the kinetic diameter of CO_2 (3.30 Å) is much smaller than that of N_2 (3.64 Å),[37] while the polyimides in this study have very small pores (ca. 5.5 Å) and quite narrow pore size distributions. The sorption selectivity effects are advantageous for the recognition of small CO_2 from the large N_2 molecule. For MPI-1, the separation factor of CO_2/N_2 is up to 102, surpassing those for zeolitic imidazole frameworks (ZIFs, 20–50),[8b] Bio-MOF-11 (81),[9c] and comparable to the amine-decorated 12-connected porous MOF CAU-1 (101)[9e] and the hierarchically porous electron-rich covalent organonitridic frameworks (PECONF-1, 109).[38]Among the three polymers, MPI-1 simultaneously possesses the higher CO_2 uptake and CO_2/N_2 selectively. Relatively, the CO_2/N_2 selectivities of MPI-2 and MPI-3 apparently decrease. Considering that the three polymers have the similar pore sizes and distributions, the main reason for their difference in CO_2/N_2 selectivity may lie in the complexity of pore channels arisen from the topological structures of the building units for the three polyimides.

For CO_2/CH_4 gas pair, things are different. The critical temperature of CH_4 gas is 191 K, which is higher than that of N_2 (126 K).[39] The previous reports have demonstrated that the gas solubility coefficient in a polymer is positively correlated with its critical temperature.[40] Therefore, for each polymer, compared to N_2 gas, CH_4 has the more strong adsorption ability with polymer skeleton, leading to the significantly higher uptake of CH_4 than N_2. Therefore, in each case, CO_2/CH_4 selectivity is considerably lower than CO_2/N_2 (Table 2). At 273 K, the CO_2/CH_4 selectivity for MPI-2 is 12, less than BILP-2 but comparable to other BILPs[15c] and some ZIFs.[8b] On the other hand, the ranking order of CO_2/CH_4 selectivities for the three polymers is different from that of CO_2/N_2. The presence

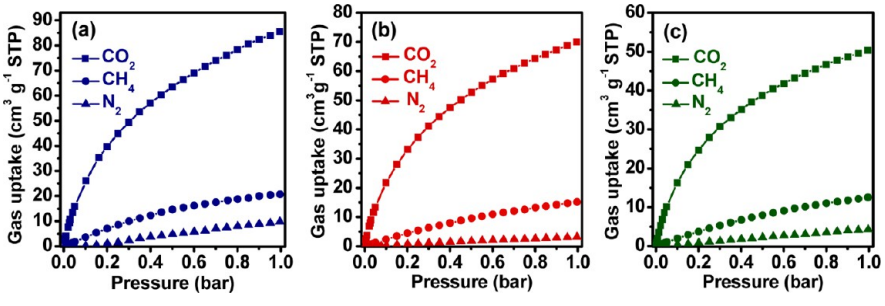

Figure 8. Adsorption isotherms of CO_2, CH_4 and N_2 gases at 273 K for MPI-1 (a), MPI-2 (b), and MPI-3 (c).

dx.doi.org/10.1021/ma400496q | Macromolecules 2013, 46, 3058–3066

of quaternary carbons may result in MPI-1 the favorable adsorption for the aliphatic CH_4 gas. As a result, the CO_2/CH_4 selectivity of MPI-1 is the lowest among the three polymers.

It is noteworthy that, in fact, the components of flue gas, natural gas and landfill gas are rather complex. In the case of flue gas, the influence of water on the CO_2/N_2 selectivity should also be considered. For a typical flue gas of post-combustion from coal-fired plants, there are about 15−16% CO_2 and 5−7% water vapor.[1] In other word, the partial pressure of CO_2 in the flue gas is about 0.15 bar, whereas that of water vapor is 0.05 bar. Therefore, from the adsorption curves of CO_2 and water vapor at 298 K (Figure 4 and Figure 5), the ratios of adsorption capacity of CO_2 at 0.15 bar to that of water vapor at 0.05 bar can be calculated. The data in Table 2 show that, for flue gas, the three samples are more preferentially adsorbed by CO_2 rather than water vapor. For example, the CO_2/H_2O ratios for MPI-1, MPI-2, and MPI-3 are 10.5, 5.5, and 10.9, respectively. Even so, the competition of adsorption between water vapor and CO_2 can not be ignored. Especially for a humidified flue gas or at the high feed pressure, the actual values of CO_2/N_2 sorption selectivity may be lower than those listed in Table 2 to some extent.

CONCLUSIONS

Three microporous polyimide networks MPI-1, MPI-2, and MPI-3 with BET surface areas in the range of 586−1454 $m^2\ g^{-1}$ have been successfully synthesized through polycondensation of pyromellitic dianhydride with tetra(4-aminophenyl)methane, 1,3,5-tris(4-aminophenyl)benzene), and tris(4-aminophenyl)-amine, respectively. Their chemical structures were confirmed by FTIR, solid-state ^{13}C CP/MAS NMR spectra, and elemental analyses. The analyses of N_2 sorption isotherms reveal that three polymers have quite narrow pore size distribution with pores centered at ca. 5.5 Å, agreeing with the observations of high-resolution TEM images. The small and uniform pore sizes were resulted from the homogeneous and random inter-penetration of network by means of elaborate control of the polymerization conditions, which process was explained with the assistance of computer modeling method. The presence of a large amount of heteroatoms results in the strong affinity of polyimide skeletons toward CO_2 molecule. Consequently, all the three polymers have high isosteric heat of adsorption above 30.0 kJ mol^{-1}. At 1.0 bar and 273 K, the high CO_2 uptake capacities as high as 16.8 wt % have been achieved. The selectivities for CO_2/N_2 and CO_2/CH_4 are up to 102, and 12, respectively, superior to many other microporous organic polymers. Furthermore, the polymers display excellent abilities to adsorb organic pollutants like benzene vapor. For MPI-1, the uptake for benzene vapor at room temperature reach 119.8 wt %, and the benzene/N_2 and benzene/H_2O selectivities are 342 and 28, respectively, which exceed most silica, inorganic−organic hybrid, and carbon materials. The above results indicate that the resulted polyimides are promising candidates as adsorbents for CO_2 capture as well as air- and water-cleaning in the environmental protection field.

ASSOCIATED CONTENT

Supporting Information

This section contains nine figures and two tables, including the FTIR and solid-state ^{13}C CP/MAS NMR spectra, X-ray diffraction patterns, TGA curves, enlarged TEM images, adsorption selectivities of CO_2 over CH_4 and N_2, and adsorption selectivities of benzene over H_2O and N_2 as well as the data of elemental analysis and virial parameters of the polyimide networks. This material is available free of charge via the Internet at http://pubs.acs.org.

AUTHOR INFORMATION

Corresponding Author

*(Z.G.W.) E-mail: zgwang@dlut.edu.cn.

Notes

The authors declare no competing financial interest.

ACKNOWLEDGMENTS

We thank the National Science Foundation of China (Nos. 51073030 and 51273031) and the Program for New Century Excellent Talents in University of China (No. NCET-06-0280) for financial support of this research.

REFERENCES

(1) D'Alessandro, D.; Smit, B.; Long, J. *Angew. Chem., Int. Ed.* **2010**, *49*, 6058−6082.
(2) Bae, Y. S.; Snurr, R. Q. *Angew. Chem., Int. Ed.* **2011**, *50*, 11586−11596.
(3) Buchard, A.; Jutz, A. F.; Kember, M. R.; White, A. J. P.; Rzepa, H. S.; Williams, C. K. *Macromolecules* **2012**, *45*, 6781−6795.
(4) Lee, E. H.; Ahn, J. Y.; Dharman, M. M.; Park, D. W.; Kim, I. L. *Catal. Today* **2008**, *131*, 130−134.
(5) Zhao, Y.; Zhang, J. *J. Nat. Gas Chem.* **2007**, *16*, 389−392.
(6) Cheng, Q.; Zhong, S. *Chin. J. Catal.* **2003**, *24*, 558−562.
(7) (a) Rochelle, G. T. *Science* **2009**, *325*, 1652−1654. (b) MacDowell, N.; Florin, N.; Buchard, A.; Hallett, J.; Galindo, A.; Jackson, G.; Adjiman, C. S.; Williams, C. K.; Shah, N.; Fennell, P. *Energy Environ. Sci.* **2010**, *3*, 1645−1669.
(8) (a) Zheng, B. S.; Bai, J. F.; Duan, J. G.; Wojtas, L.; Zaworotko, M. J. *J. Am. Chem. Soc.* **2011**, *133*, 748−751. (b) Banerjee, R.; Furukawa, H.; Britt, D.; Knobler, C.; O'Keeffe, M.; Yaghi, O. M. *J. Am. Chem. Soc.* **2009**, *131*, 3875−3877. (c) Yang, S. T.; Kim, J. Y.; Kim, J.; Ahn, W. S. *Fuel* **2012**, *97*, 435−442. (d) McEwen, J.; Hayman, J. D.; Yazaydin, A. O. *Chem. Phys.* **2013**, *412*, 72−76. (e) Pham, T. D.; Liu, Q. L.; Lobo, R. F. *Langmuir* **2013**, *29*, 832−839.
(9) (a) Vaidhyanathan, R.; Iremonger, S. S.; Dawson, K. W.; Shimizu, G. K. H. *Chem. Commun.* **2009**, 5230−5232. (b) Couck, S.; Denayer, J. F. M.; Baron, G. V.; Rémy, T.; Gascon, J.; Kapteijn, F. *J. Am. Chem. Soc.* **2009**, *131*, 6326−6327. (c) An, J. H.; Geib, S. J.; Rosi, N. L. *J. Am. Chem. Soc.* **2010**, *132*, 38−39. (d) Si, X. L.; Jiao, C. L.; Li, F.; Zhang, J.; Wang, S.; Liu, S.; Li, Z. B.; Sun, L. X.; Xu, F.; Gabelica, Z.; Schick, C. *Energy Environ. Sci.* **2011**, *4*, 4522−4527.
(10) (a) Li, J. R.; Kuppler, R. J.; Zhou, H. C. *Chem. Soc. Rev.* **2009**, *38*, 1477−1504. (b) Panda, T.; Pachfule, P.; Chen, Y.; Jiang, J.; Banerjee, R. *Chem. Commun.* **2011**, *47*, 2011−2013. (c) Weber, J.; Du, N. Y.; Guiver, M. D. *Macromolecules* **2011**, *44*, 1763−1767. (d) Arstad, B.; Fjellvag, H.; Kongshaug, K. O.; Swang, O.; Blom, R. *Adsorption* **2008**, *14*, 755−762.
(11) (a) Yuan, D. Q.; Lu, W. G.; Zhao, D.; Zhou, H. C. *Adv. Mater.* **2011**, *23*, 3723−3725. (b) Furukawa, H.; Yaghi, O. M. *J. Am. Chem. Soc.* **2009**, *131*, 8875−8883.
(12) Dawson, R.; Stöckel, E.; Holst, J. R.; Adams, D. J.; Cooper, A. I. *Energy Environ. Sci.* **2011**, *4*, 4239−4245.
(13) (a) Lu, W. G.; Yuan, D. Q.; Sculley, J.; Zhao, D.; Krishna, R.; Zhou, H. C. *J. Am. Chem. Soc.* **2011**, *133*, 18126−18129. (b) Lu, W. G.; J. Sculley, P.; Yuan, D.; Krishna, Q. R.; Wei, Z. G..; Zhou, H. C. *Angew. Chem., Int. Ed.* **2012**, *51*, 7480−7484.
(14) (a) Katsoulidis, A. P.; Kanatzidis, M. G. *Chem. Mater.* **2011**, *23*, 1818−1824. (b) Katsoulidis, A. P.; Kanatzidis, M. G. *Chem. Mater.* **2012**, *24*, 471−479.
(15) (a) Rabbani, M. G.; El-Kaderi, H. M. *Chem. Mater.* **2012**, *24*, 1511−1517. (b) Rabbani, M. G.; Reich, T. E.; Kassab, R. M.; Jackson, K. T.; El-Kaderi, H. M. *Chem. Commun.* **2012**, *48*, 1141−1143. (c) Zhao, Y. C.; Cheng, Q. Y.; Zhou, D.; Wang, T.; Han, B. H. *J.*

Mater. Chem. **2012**, *22*, 11509−11514. (d) Yu, H.; Tian, M. Z.; Shen, C. J.; Wang, Z. G. *Polym. Chem.* **2013**, *4*, 961−968.
(16) (a) Yu, H.; Shen, C. J.; Tian, M. Z.; Qu, J.; Wang, Z. G. *Macromolecules* **2012**, *45*, 5140−5150. (b) Yu, H.; Shen, C. J.; Wang, Z. G. *ChemPlusChem* **2013**, DOI: 10.1002/cplu.201300090.
(17) Wang, X. S.; Liu, J.; Bonefont, J. M.; Yuan, D. Q.; Thallapally, P. K.; Ma, S. Q. *Chem. Commun.* **2013**, *49*, 1533−1535.
(18) Robeson, L. M.; Langsam, M. *Sep. Sci. Technol.* **1992**, *27*, 1245−1258.
(19) (a) Weber, J.; Su, Q.; Antonietti, M.; Thomas, A. *Macromol. Rapid Commun.* **2007**, *28*, 1871−1876. (b) Ghanem, B. S.; McKeown, N. B.; Budd, P. M.; Al-Harbi, N. M.; Fritsch, D.; Heinrich, K.; Starannikova, L.; Tokarev, A.; Yampolskii, Y. *Macromolecules* **2009**, *42*, 7881−7888. (c) Wang, Z. G.; Zhang, B. F.; Yu, H.; Sun, L. X.; Jiao, C. L.; Liu, W. S. *Chem. Commun.* **2010**, *46*, 7730−7732. (d) Wang, Z. G.; Zhang, B. F.; Yu, H.; Li, G. Y.; Bao, Y. J. *Soft Matter* **2011**, *7*, 5723−5730. (e) Luo, Y.; Li, B.; Liang, L.; Tan, B. *Chem. Commun.* **2011**, *47*, 7704−7706. (f) Rao, K. V.; Haldar, R.; Kulkarni, C.; Maji, T. K.; George, S. J. *Chem. Mater.* **2012**, *24*, 969−971. (g) Shen, C. J.; Bao, Y. J.; Wang, Z. G. *Chem. Commun.* **2013**, *49*, 3321−3323.
(20) Miller, R. D.; Burland, D. M.; Jurich, M.; Lee, V. Y.; Moylan, C. R.; Thackara, J. I.; Twieg, R. J.; Verbiest, T.; Volksen, W. *Macromolecules* **1995**, *28*, 4970−4974.
(21) (a) Hu, Z. G.; Liu, J.; Li, G. A.; Dong, Z. B.; Li, W. *J. Chin. Chem. Soc.* **2004**, *51*, 581−583. (b) Yeh, R. M.; Xu, J.; Seeber, G.; Raymond, K. N. *Inorg. Chem.* **2005**, *44*, 6228−6239.
(22) (a) Dawson, R.; Laybourn, A.; Clowes, R.; Khimyak, Y. Z.; Adams, D. J.; Cooper, A. I. *Macromolecules* **2009**, *42*, 8809−8816. (b) Stöckel, E.; Wu, X. F.; Trewin, A.; Wood, C. D.; Clowes, R.; Campbell, N. L.; Jones, J. T. A.; Khimyak, Y. Z.; Adams, D. J.; Cooper, A. I. *Chem. Commun.* **2009**, *2*, 212−214.
(23) Zhang, B. F.; Wang, Z. G. *Chem. Mater.* **2010**, *22*, 2780−2789.
(24) Lillo-Ródenas, M. A.; Cazorla-Amorós, D.; Linares-Solano, A. *Adsorption* **2011**, *17*, 473−481.
(25) Zhang, J. P.; Chen, X. M. *J. Am. Chem. Soc.* **2008**, *130*, 6010−6017.
(26) Tilford, R.; Mugavero, W. S. J., III; Pellechia, P. J.; Lavigne, J. J. *Adv. Mater.* **2008**, *20*, 2741−2746.
(27) Holst, J. R.; Stöckel, E.; Adams, D. J.; Cooper, A. *Macromolecules* **2010**, *43*, 8531−8538. (b) Dawson, R.; Adams, D. J.; Cooper, A. *Chem. Sci.* **2011**, *2*, 1173−1177.
(28) (a) McKeown, N. B.; Budd, P. M. *Macromolecules* **2010**, *43*, 5163−5176. (b) Thomas, A. *Angew. Chem., Int. Ed.* **2010**, *49*, 8328−8344. (c) Wu, D. C.; Xu, F.; Sun, B.; Fu, R. W.; He, H. K.; Matyjaszewski, K. *Chem. Rev.* **2012**, *112*, 3959−4015.
(29) Krungleviciute, V.; Heroux, L.; Migone, A. D. *J. Phys. Chem. B.* **2005**, *109*, 9317−9320.
(30) Cole, J. H.; Everett, D. H.; Marshall, C. T.; Paniego, A. R.; Powl, J. C.; Rodriguez-Reinoso, F. *J. Chem. Soc., Faraday Trans.* **1974**, *70*, 2154−2169.
(31) Martín, C. F.; Stöckel, E.; Clowes, R.; Adams, D. J.; Cooper, A.; Pis, J. J.; Rubiera, F.; Pevida, C. *J. Mater. Chem.* **2011**, *21*, 5475−5483.
(32) Rabbani, M. G.; El-Kaderi, H. M. *Chem. Mater.* **2011**, *23*, 1650−1653.
(33) (a) Jackson, K. T.; Rabbani, M. G.; Reich, T. E.; El-Kaderi, H. M. *Polym. Chem.* **2011**, *2*, 2775−2777. (b) Reich, T. E.; Behera, S.; Jackson, K. T.; Jena, P.; El-Kaderi, H. M. *J. Mater. Chem.* **2012**, *22*, 13524−13528.
(34) (a) Demessence, A.; D'Alessandro, D. M.; Foo, M. L.; Long, J. R. *J. Am. Chem .Soc.* **2009**, *131*, 8784−8786. (b) Fu, Y. H.; Sun, D. R.; Chen, Y. J.; Huang, R. K.; Ding, Z. X.; Fu, X. Z.; Li, Z. H. *Angew. Chem., Int. Ed.* **2012**, *51*, 3364−3367.
(35) Yu, L.; Falco, C.; Weber, J.; White, R. J.; Howe, J. Y.; Titirici, M. M. *Langmuir* **2012**, *28*, 12373−12383.
(36) (a) An, J.; Geib, S. J.; Rosi, N. L. *J. Am. Chem. Soc.* **2010**, *132*, 38−39. (b) Banerjee, R.; Furukawa, H.; Britt, D.; Knobler, C.; O'Keeffe, M.; Yaghi, O. M. *J. Am. Chem .Soc.* **2009**, *131*, 3875−3877.
(37) Breck, D. W. *Zeolite Molecular Sieves*; John Wiley & Sons: New York, 1994.
(38) Mohanty, P.; Kull, L. D.; Landskron, K. *Nat. Commun.* **2011**, *2*, 1−6.
(39) Jeans, J. *An Introduction to the Kinetic Theory of Gases*; Cambridge University Press: London, 1982.
(40) (a) Amerongen, G. J. *J. Appl. Phys.* **1946**, *17*, 972−986. (b) Suwandi, M. S.; Stern, S. A. *J. Polym. Sci., Polym. Phys. Ed* **1973**, *11*, 663−681. (c) Shah, V. M.; Hardy, B. J.; Stern, S. A. *J. Polym. Sci., Polym. Phys. Ed.* **1986**, *24*, 2033−2047.